Coal matrix pores analysis using nano-scale SEM and direct capillary pressure curves simulation

Alexandra Roslin[a]，Dubravka Pokrajac[a]，Yingfang Zhou[*]

[a] School of Engineering, University of Aberdeen, Aberdeen, AB243UE, United Kingdom

Abstract

This paper presents an analysis of matrix pore size distribution and simulation of fluid flow in the coal matrix in intermediate rank coal. The study utilised scanning electron microscopy (SEM) images, nuclear magnetic resonance (NMR) and mercury injection capillary pressure (MICP) data which were used to reconstruct the 3D coal matrix model and to analyse the distribution of pores in coal matrix. Reconstructed 3D model of coal matrix pore space was further utilised to simulate capillary dominated two-phase flow for capillary pressure curves and fluid configuration calculation. The analysis showed that there is a good congruence between the simulated and measured MICP curves, which could mean that the described simulation method could potentially be used for modelling of fluid flow in coal. Simulation approach which was described in the paper can potentially be implemented to model fluid flow in dual-pore single-permeability or dual-pore dual-permeability models. Results confirm that the contribution of the coal matrix to the permeability and fluid flow is negligible due to the poor connectivity of the pore system in the coal matrix of the studied samples.

Keywords

Nano-Scale SEM; Capillary pressure curves; Level-set method; Coal matrix

Introduction

Pore and fractures are important morphological features of the coal matrix and provide not only the main storage but also important conduits for coal bed methane production (Fang et al., 2019). Based on the pore diameter, pores can be classified as supermicropores (<2nm), micropores (2-10nm), mesopores (10-100nm), macropores (100-1000nm), supermacropores (10^3-10^4nm) and microfractures (>10^4nm) (Hodot, 1966; Cai et al., 2013). Different factors control the size and volume of pores in coal (Mastalerz et al., 2008) amongst which coal rank is one of the most important. It was previously observed (Gan et al., 1972; Clarkson and Bustin, 1996) that medium volatile bituminous rank and higher coal micropores are the main contributors to the total porosity, while for high volatile bituminous rank coal the bulk of porosity represented by micropores and mesopores. In turn, in subbituminous rank and below coal macroporosity is dominant. Pore volume and pore size distribution are also influenced by maceral composition. It was generally observed that the pore surface area increases with increased vitrinite content (e.g. Thomas and Damberger, 1976). It was

concluded based on the study of different coal samples that vitrinite to be micro- and mesoporous, inertinite mostly mesoporous, and liptinite is the least porous coal maceral (Harris and Yust, 1979; Unsworth et al., 1989; Lamberson and Bustin, 1993; Clarkson and Bustin, 1996).

The prevailing conception in coal geology states that the cleat network offers the permeability for fluid flow while matrix pores have negligible contribution if any (Clarkson and Bustin, 1996; Moore, 2012; Puri et al., 1991). Previous researchers (e.g. Karacan and Okandan, 2000) modelled gas flow in pores in two phases: absorbed gas in coal matrix diffuses to the coal cleats, and then viscous flow in cleat network becomes dominant (Giffin et al., 2013). However, in the current research, it was decided to analyse whether coal matrix porosity can also contribute to viscous flow, thus increasing cleat permeability. There are different methods to simulate flow in porous space (Blunt at al., 2013). One of the popular approaches is the lattice Boltzmann method (e.g. Chen and Doolen, 1998) which is one of the particle-based methods, where particles representing packets of fluid are tracked through the flow domain used for computations (Blunt et al., 2013). There are also other techniques designed mostly to simulate capillary-controlled displacement. For example, for the current research, the level-set method can demarcate an interface between fluids and model its propagation in a quasi-static displacement (Sussman et al., 1994; Prodanovic et al., 2010). The main advantage of this method is that the complex boundaries between fluids can be handled naturally, and there are no constraints on the topology of the interface.

Orthogonal nano-scale SEM images were used to reconstruct a 3D piece of coal sample suitable for fluid flow simulation to determine the computational flow domain. SEM technology is widely used 2D imaging method for pore distribution and morphology analysis (e.g. Giffin et al., 2013). Still, in the course of the current research, it was also used for 3D reconstruction using statistical methods. For the research described in this paper, the stochastic pore space reconstruction approach which is based on Markov chain method (Wu et al., 2006) is adopted to reconstruct 3D images from 2D nano-scale SEM image. Generally, this method is based on the idea of using a small number of local features to predict global conditions based on available 2D or 3D images (Wu et al., 2004). This approach takes into account the relationship between several near neighbours to generalise the features of the porous medium. This method was previously successfully implemented to reconstruct both homogeneous and heterogeneous samples and also allowed to analyse the reconstructed porous medium quantitatively, and it demonstrated good results for the studied coal (Roslin et al., in press). The research described in this paper focused on the analysis of the multiphase flow simulation in the matrix pore space based on the reconstructed 3D model. The approach which was implemented in

the current research considers direct modelling of fluid flow using the level-set method as it is explained below.

Input data

A sample of intermediate rank coal from Southern Qinshui Chinese coal bed methane basin was obtained and examined using nano-scale SEM technology. The main characteristics of the analysed coal sample acquired from coal proximate analysis are listed in Table 1.

Table 1. Coal sample characteristics.

Sample ID	Sample (%)			Organic matter (%)			Vitrinite Reflectance$^{o}_{ran}$ (%)
	Organic matter	Pyrite	Others	Vitrinite	Inertinite	Liptinite	
PL3#-2	79.87	0.17	19.97	77.52	22.48	0.00	1.68

Previous studies (e.g. Wang et al., 2016; Cai et al., 2011) show that the coal from this basin contains 0.59 – 3.54% moisture, 3.5 – 15.54% ash yield, 73.62 – 88.92% fixed carbon and 2.14 – 4.04% hydrogen, with C/H ratios in the range of 19.96 – 36.25. The vitrinite reflectance ranges from 1.95 to 3.49%.

For the research, the sample was divided into two pieces: the upper part of the sample was used to perform NMR (nuclear magnetic resonance) and later MICP (mercury injection capillary pressure). This part of the sample was also divided into two pieces, cut, polished in three perpendicular to each other directions and carbon-coated (Figure 1). This was required to obtain SEM data in three directions for better 3D reconstruction of pore space. The lower part of the sample was also used for NMR and MICP laboratory experiments, but it was not implemented into SEM analysis.

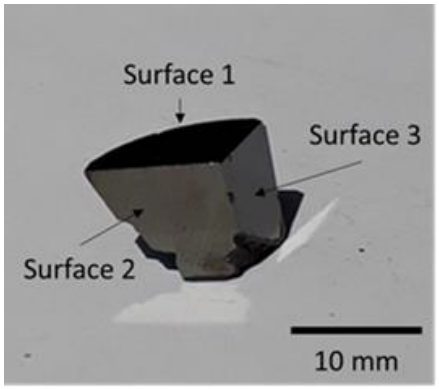

Figure 1. Coal core sample polished and carbon-coated for SEM analysis.

Methodology

First of all, the samples were scanned using SEM microscopy, and ZEISS Gemini EVO MA10 SEM Microscopy was exploited to obtain the images of the nanoscale under high vacuum condition (magnification range of x20 – x50,000). For the current research, these images were exploited to reconstruct several 3D cubes (Roslin et al., in press) which contained 400^3 voxels using the previously established stochastic algorithm (Wu et al., 2006). It is an iterative algorithm which decides the state of each pixel (matrix or pore) based on the knowledge about the state of the neighbouring pixels (Wu et al., 2004). Reconstructed 3D cubes (with the resolution of the cubes between 6 and 28 nm) were then used to extract pore network and to analyse the flow and to simulate pressure curves using a network simulator developed by Ahmed Boujelben at Heriot-Watt University (https://github.com/ahboujelben/numSCAL_basic). Simulation of the capillary pressure curves demonstrated that there is a big discrepancy between simulated and MICP pressure curves (Roslin et al., in press). The reconstructed model was then exploited for simulation of fluid flow using direct pore-scale modelling using the level-set method as it is explained below.

Capillary dominated primary drainage were performed in the reconstructed 3D coal sample using the contact angle level-set method (Jettestuen et al., 2013). The level set method was initially introduced by Osher and Sethian (1988) to explicitly track interface where the level set function equals to 0. This method was initially adopted by Prodanović and Bryant (2006) to model critical displacements events during drainage and imbibition as well as complete capillary pressure curves in 3D rock images (Prodanović and Bryant, 2009; Prodanović et al., 2010) at the strongly water-wet condition. It was then extended to include contact angle, define at the three-phase contact line, to investigate the wettability on fluid distribution and capillary pressure curves in 3D rock images (Jettestuen et al., 2013). In this method, two level-set functions, ψ and ϕ, are used to represent the solid and fluid, respectively. A sketch of the simulation setup is shown in Figure 2. As shown in this figure, the shaded regions represent the solid, $\psi = 0$ represents the pore boundary, and $\phi = 0$ denotes the interface between wetting and non-wetting phase, θ is the contact angle defined at the three-phase contact point. And $\beta = \pi - \theta$ is defined as the angle between the surface normal of ψ and ϕ at the contact point.

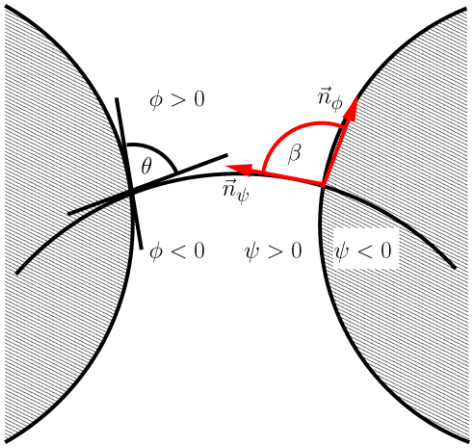

Figure 2. The figure shows an illustration of the setup. The shaded regions represent the solid, $\boldsymbol{\psi = 0}$ represents the pore boundary, and $\boldsymbol{\phi = 0}$ denotes the interface between wetting and non-wetting phase, θ is the contact angle defined at the three-phase contact point (adopted from Jettestuen et al., 2013).

For a given capillary pressure, $P_c = \sigma\kappa_0$ (σ is the surface tension and κ_0 is the interface curvature), the equilibrium fluid configuration is obtained by solving numerically the evolution equation of the level set function with velocity contribution from normal, advective and diffusive/parabolic term as given in Eq. (1) (Jettestuen et al., 2013),

$$(\phi)_t + H(\psi)(\kappa_0 - \kappa_\phi)|\nabla\phi| + H(-\psi)S(\psi)(\nabla\psi \cdot \nabla\phi - \cos\beta|\nabla\psi||\nabla\phi|) = 0 \qquad (1)$$

where κ_ϕ is the curvature of the level sets, H is the Heaviside step function defined as,

$$H(x) = \begin{cases} 0 & x < -\varepsilon, \\ \frac{1}{2} + \frac{x}{2\varepsilon} + \frac{x}{2\pi}\sin\left(\frac{\pi x}{\varepsilon}\right) & -\varepsilon \le x \le \varepsilon, \\ 1 & x > \varepsilon, \end{cases} \qquad (2)$$

and S is the signed distance function defined by:

$$S(x) = \frac{x}{\sqrt{x^2 + |\nabla x|^2 (\Delta x)^2}} \qquad (3)$$

Capillary controlled fluid displacements in the reconstructed 3D coal sample are simulated by solving equation (1) until steady-state is achieved for a given interface curvature, κ_0. The numerical algorithm is the parallelized by OpenMPI to allow more considerable size computation. The detailed numerical implementation could be found in Jettestuen et al., (2013). The wetting phase saturation at the given interface curvature, κ_0, is then estimated by:

$$S_w = \frac{\int_{\Omega} H(\psi) H(\phi) dV}{\int_{\Omega} H(\psi) dV} \quad (3)$$

Where *V* is the volume of the sample, and the non-wetting phase, e.g., mercury, saturation (S_m) is obtained by $S_m = 1 - S_w$.

The full mercury injection capillary pressure curves are simulated by change the fluids interface curvature, κ_0, stepwise until the wetting phase (air) saturation reaches 0.05, or the maximum capillary pressure reaches 200 MPa.

Mercury injection capillary pressure (MICP) method is typically used to understand the relationship between capillary pressure and the porous structure of the sample (Purcell, 1949). In MICP the pores of the sample are emptied (usually by drying the sample) and then filled with mercury with increasing pressure. The volume of mercury at each given pressure is recorded, and the resulting capillary pressure curves can be compared to the modelled pressure curves.

Results

In the course of the current research, an intermediate rank coal sample was analysed using SEM technologies with the support of NMR and MICP data to determine pore size distribution. Histogram of NMR analysis pore size distribution demonstrated two distinctive peaks about 1nm and 1 micron (Figure 3). MICP data are in conjunction with NMR data and shows that the majority of pores are smaller than 25 nm or bigger than 1 micron (Figure 4). However, MICP data also demonstrated that there is some noticeable percentage of pores in the range of 25–100 nm. These results are congruent with the outcome of the SEM reconstructed model (Figure 5), which shows that the majority of pores are in the range 40-70nm and throats are in the range 10-50nm. So, according to a combined classification from IUPAC (IUPAC, 1982) and Hodot (Hodot, 1966) for coal pore size, the pore system is mostly presented by micropores and mesopores, but some distinctive amount of macropores and microfractures were also observed. Those pores are elongated (Figure 6).

The results obtained for coal samples from other regions predicted that the studied coal should contain mostly micropores but may have some amount of mesopores. The assessment of pore size distribution is in good conjunction with these observations.

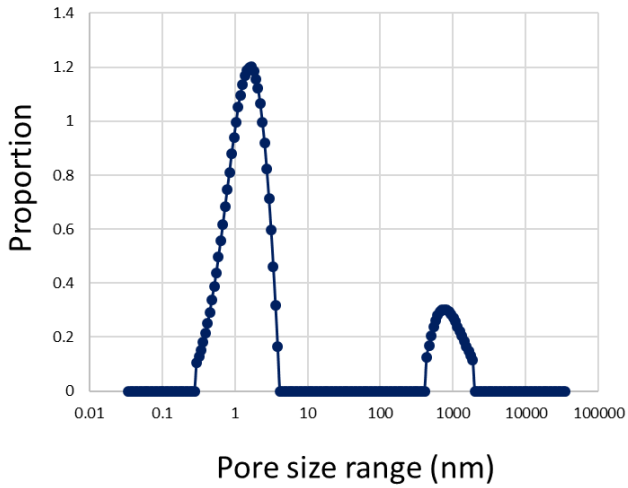

176

177 Figure 3. Pore size distribution obtained from NMR analysis.

178

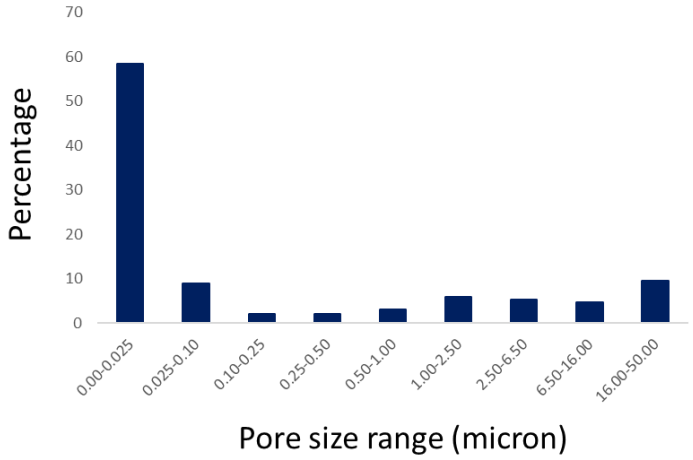

179

180 Figure 4. Pore size distribution obtained from MICP data.

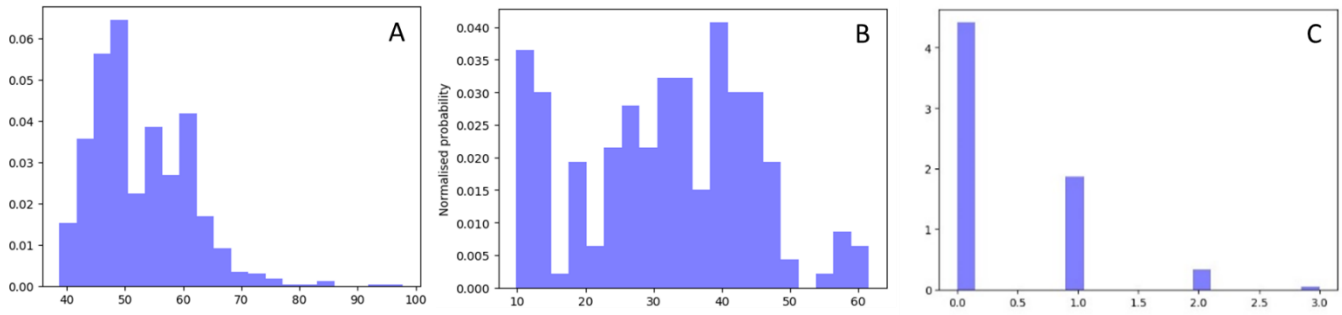

181

182 Figure 5. Pore size (A), throat size (B) distribution and coordination number (C) obtained from the

183 reconstructed 3D model (Roslin et al., in press).

184

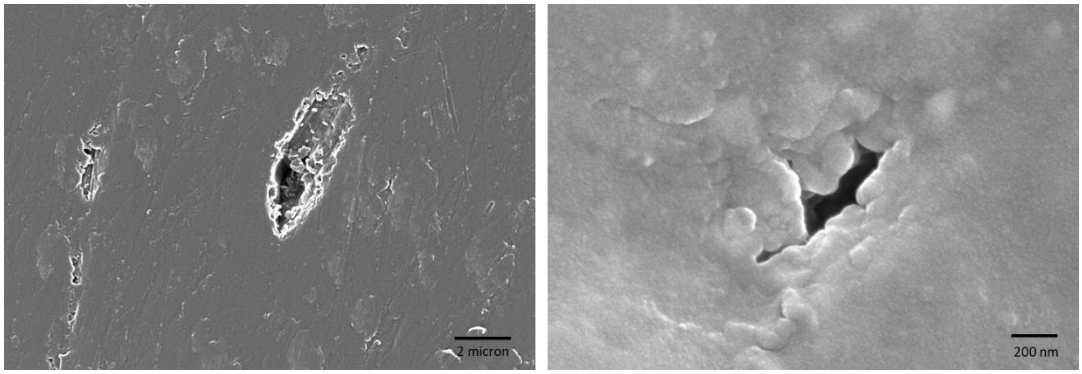

Figure 6. Example of SEM image with pores at a different magnification.

Another critical issue related to the matrix pores was to estimate the connectivity of pores and especially, the connectivity of macropores and microfractures. Those macropores and microfractures might have a significant contribution to fluid flow if they were connected. The microfractures were beyond the resolution of micro-CT scanner because of their size (length <10 microns and width <100 nm). Some microscopic sections were made in different directions and analysed to estimate the connectivity of the microfractures. Detailed microscopy scanning analysis of microfractures distribution and propagation demonstrated that the fractures do not form any connected network system and are rather isolated in a 3D space. Analysis of the statistics (Figure 5) of the reconstructed 3D model revealed that most of the pores are connected to one or less than one neighbour, and only little amount of pores has two or more connections. Also, no clear relationship between pore size and connectivity was observed, i.e. micropores, mesopores and macropores have very similar connectivity numbers (Figure 7).

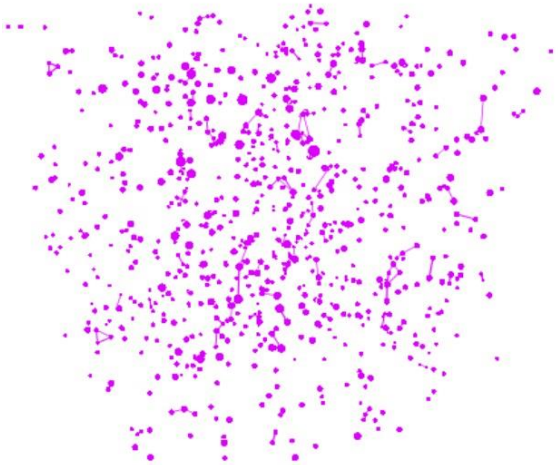

Figure 7. Extracted pore network for the reconstructed 3D model (model size is 8*8*8 micron).

After the statistical analysis of pore size distribution and connectivity, the main conclusion was that the matrix pores do not contribute to the fluid flow and coal permeability. However, NMR and MICP

analysis demonstrated that a massive portion of pores is in the range between 0.5 and 5nm, that is beyond the resolution of SEM images. To estimate whether these pores have a significant contribution to the fluid flow, we performed fluid flow simulation on the reconstructed 3D model and compared the resulting capillary pressure curves to MICP pressure curves to estimate whether there is any discrepancy.

The capillary pressure curve for the reconstructed 3D coal sample is simulated using the contact angle level-set method as described above. The contact angle, θ, is given as 40° and the surface tension between mercury and air is set as 400mN/m.

The results are demonstrated in Figure 8. Figure 8 shows that the fluid occupies only a small portion of pores and then the process of mercury sorption stops.

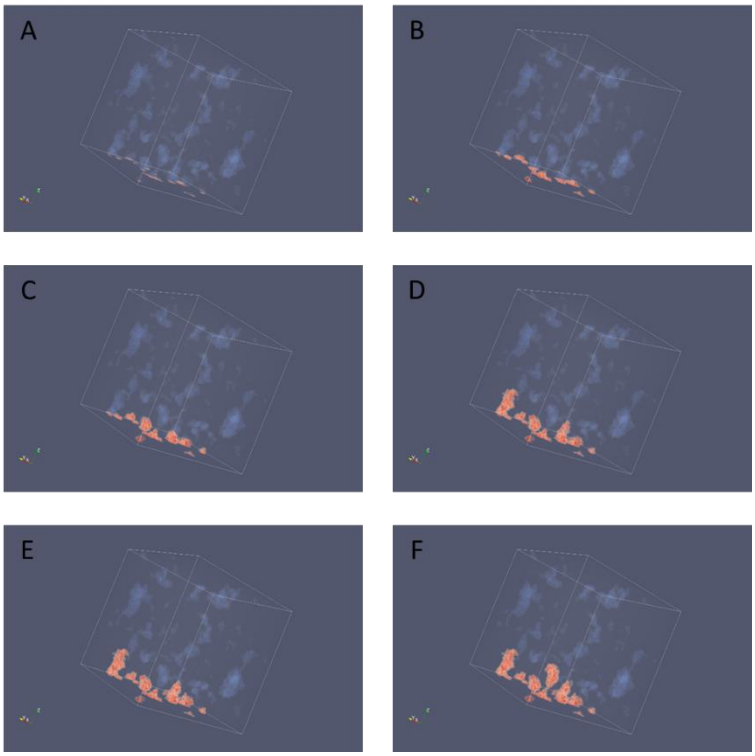

Figure 8. Fluid configuraton simulated at different capillary pressures: A) Pc=0.01 MPa; B) Pc=0.96 MPa; C) Pc=14 MPa; D) Pc=20 MPa; E) Pc=30 MPa; F) Pc=55 MPa. Blue colour represents wetting phase, red colour represents non-wetting phase.

Figure 9 demonstrates the comparison of simulated and MICP pressure curves. As can be seen, there is a reasonable congruence between the simulated and MICP curves. The observed congruence is particularly important because the previous pore network simulation (Roslin et al., in press)

demonstrated a significant discrepancy between simulated and MICP curves. However, the observed discrepancy of current simulation results should be assessed and explained in detail.

Figure 9 demonstrates three main zones which can be highlighted in Figure 9. The main difference between simulated and MICP curves is observed in zone 1, where the simulated curve is more abrupt compared to the MICP curve. A graduate increase of capillary pressure characterises this zone. For the current research, the drainage process (non-wetting phase replaces the wetting phase) is simulated. So it can be concluded that big pores are invaded by mercury at low pressures, then, when the pressure increases, the small pores are also invaded. As can be seen, mercury saturation increases gradually in case of laboratory data and abruptly in case of simulated data. It can probably be explained by the fact that images used for 3D model reconstructions had only a few macropores and microfractures, which then does not contribute much to mercury saturation in case of simulation. These big pores were invaded very quickly, and the simulated curve reached the plateau (zone 2) earlier than the MICP curve. Plateau zone is more significant for the simulated curve, which can be explained by the fact that the 3D model contained mostly mesopores which are responsible for the mercury saturation. In turn, zone 3 probably reflects the presence of some minor amount of micropores in the reconstructed model, which are invaded at the last stage of the drainage process. The pore size distribution analysis also supports the conclusion that the discrepancy between the simulated and the laboratory pressure curves in zone 2 may be caused by the fact that mostly mesopores were included in the reconstructed model. This analysis demonstrated that the size of pores determined from the reconstructed model is about 2-3 times bigger than the size of pores determined by mercury porosimetry data. The obtained results are discussed in the next section of the paper.

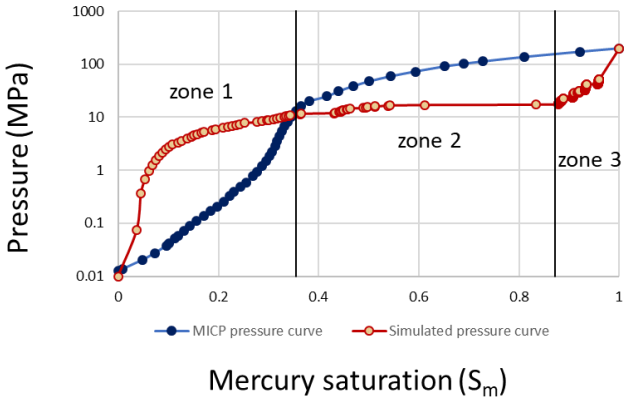

Figure 9. Level set simulation of mercury injection capillary pressure curves. Mercury saturation equal to 1 means that the whole amount of invaded pores is occupied by mercury.

Discussion

Contribution of the coal matrix pore system is usually considered to be negligible if any (Clarkson and Bustin, 1996). However, it is possible to assume that in the case of matrix pore connectivity, the matrix can no longer be ignored (Flores, 2014) (see Figure 10).

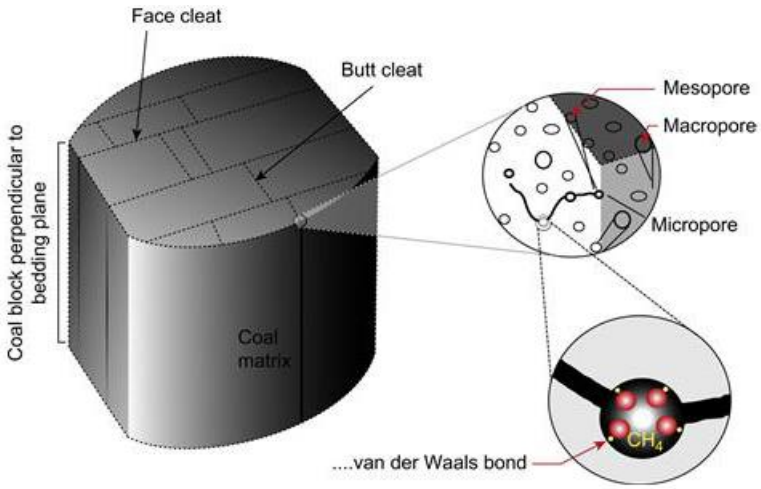

Figure 10. Diagram showing pore distribution and connectivity in the coal matrix, and adsorbed methane in a micropore (Flores, 2014).

SEM analysis of coal sample surface demonstrated that the studied sample contains some amount of microfractures (Figure 11) which means that coal matrix may have some contribution to fluid flow. The intermediate coal sample has been cut in different directions and scanned using SEM technology to check whether this assumption is correct. SEM images showed that some microfractures were elongated and formed some sort of canals in the body of the coal matrix (Figure 11). Since it was not possible to perform 3D scanning of the samples with the desired resolution, it was decided to cut the sample in different directions and to perform as many SEM scans as it was required to reconstruct representative volumes for the studied sample. As a result, five different 3D models were built based on the SEM images from different parts of the sample: some parts of the sample contained mostly micropores and mesopores, while some other parts also had macropores and microfractures. However, the analysis of pore size distribution demonstrated almost identical histograms for all five models, which means that macropores and microfractures made the minority of matrix pores.

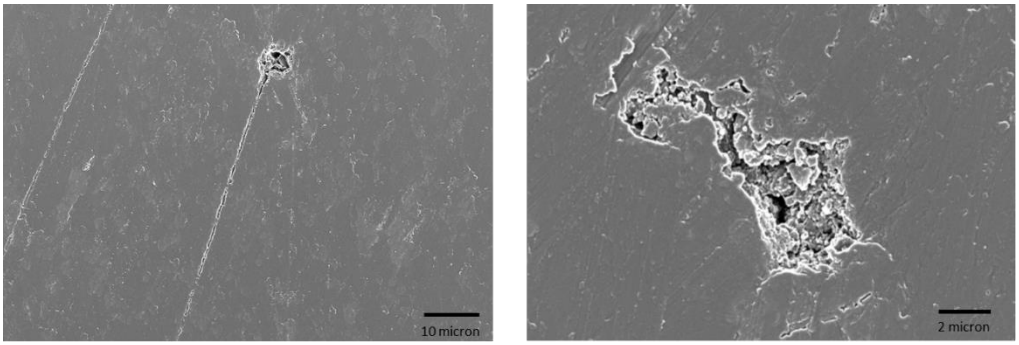

Figure 11. Example of SEM images at a different resolution.

Matrix pore connectivity was another parameter which needed to be estimated in the course of the research. Analysis of pore connectivity statistics revealed that the majority of pores are connected to less than two neighbours, and almost half of all pores are not connected at all. It means that even in the presence of a large number of pores and microfractures, they don't contribute to the fluid flow in matrix and permeability. The origin of the matrix pores can probably explain the poor connectivity of coal matrix pores. Although the origin of pores is not yet wholly understood except that they are likely to be inherited from the original peat structures or formed during coalification (Flores, 2014). Thus, macropores are probably voids of residual cell structures of precursor plants (Lin, 2010; Zhang et al., 2010; Wildman and Derbyshire, 1991) and mesopores are very similar to the macropores in origin (Zhang, 2001). In turn, the micropores possibly resulted from gelification of organic matter during coalification and compression of some large pores to smaller pores (Clarkson and Bustin, 1996; Marsh, 1987; Zhang, 2001).

Analysis of pore size distribution and connectivity led to the conclusion that coal matrix pore network doesn’t contribute to the fluid flow. However, the conclusion was made based on the 3D reconstructed model. It was decided to perform fluid flow modelling on the reconstructed pore network and compare to the MICP pressure curves to confirm this conclusion. The comparison showed a correlation between the two pressure curves. As it was shown the discrepancy between the simulated and MICP pressure curves could probably be explained by the fact that the simulated curve was built on statistically reconstructed pore network model which did not contain all the variety of pores in the sample. For the current research, that was not critical because it was not planned to reconstruct the model which would replicate the exact structure of the coal matrix but to estimate the potential contribution of the coal matrix pores into the fluid flow especially in the presence of macropores and microfractures. If it is required to reconstruct the internal structure of the coal matrix, it is recommended to utilise more SEM images for 3D reconstruction to increase the reconstructed volume of investigation. It is also desired to use not three orthogonal surfaces for SEM analysis, but more surfaces made at different angles to improve the predictive ability of modelling.

Although the contribution of the coal matrix pores to the total permeability of the studied coal sample was negligible, the current paper demonstrated that free fluid flow in coal matrix may take place to some extent, especially if micro-fractures are present. It is well-known that the fluid still propagates through the coal matrix but mostly by diffusion. If micro-fractures and macro-pores are present in coal matrix, it can be assumed that a combination of free fluid flow and diffusion takes place in coal matrix. The approach presented in the paper could therefore be important for understanding the mechanisms of fluid flow in coal, and for combining free fluid flow and diffusion simulation into a single model for flow characterisation of coals.

Another consideration which should be taken into account working with the coal samples is the applicability of mercury injection. For the current research, mercury injection was suitable because of two factors: first of all, the studied samples represented the coal of intermediate rank which was characterised by quite a significant amount of mesopores, and some amount of macropores and microfractures. It was demonstrated that mercury could invade those pores without breaking the sample. In the case of high-rank coal, mercury injection capillary pressure can be too high (since micropores present the majority of pores) and the sample can be broken.

Conclusion

In this paper, we present a systematic study of pore size distribution and capillary pressure curves modelling in coal matrix. The main conclusion of the research described in this paper is that, for the studied sample of intermediate rank coal, the pore matrix network doesn't make any significant contribution to free fluid flow. The hypothesis that the pore network of coal matrix may have a negligible contribution to the permeability of coal was previously expressed in the literature (e.g. Clakston and Bustin, 1996). However, it was also anticipated that the presence of relatively large microfractures observed under the microscope might create additional canals for fluid flow. Connectivity analysis and fluid flow simulation proved that the above hypothesis is correct for the studied samples and demonstrated that although some fluid flow may take place, poor connectivity doesn't allow fluid to propagate deep into the coal matrix. However, the paper also demonstrates that free fluid flow takes place in coal matrix to some extent, which means that it may be required in future to work on a modelling approach which will combine Darcy's flow and diffusion simulation in order to improve the understanding of the behaviour of fluids in coal reservoirs.

Acknowledgement

This paper utilised opportunistic coal samples and characterisation data as a part of a study into multiphase flow in coal for Southern Qinshui coal basin. The measurement of this work was supported by the Royal Society Edinburgh through the National Natural Science Foundation of China Cost Share Project, and Alexandra Roslin thanks the Ministry of Education of Russia to support her PhD work at the University of Aberdeen. The School of Engineering and School of Geosciences at the University of Aberdeen are thanked for their support.

Literature list

1. Blunt M. J., Bijeljic B., Dong H., Gharbi O., Iglauer S., Mostaghimi P., Paluszny A., Penland C., 2013. Pore-scale imaging and modelling. Advanced in Water Resources 51, 197-216.
2. Cai Y., Liu D., Yao Y., Li J., Qiu Y., 2011. Geological controls on prediction of coalbed methane of No. 3 coal seam in Southern Qinshui Basin, North China. International Journal of Coal Geology 88, 101 – 112.
3. Cai Y., Liu D., Pan Z., Yao Y., Li J., Qui Y., 2013. Pore structure and its impact on CH_4 adsorption capacity and flow capability of bituminous and subbituminous coals from Northeast China. Fuel 103, 258 – 268.
4. Chen S., Doolen G. D., 1980. Lattice Boltzmann method for fluid flows. Annual Review of Fluid Mechanics, 30, pp 329 – 364.
5. Clarkson C. R., Bustin R. M., 1996. Variation in micropore capacity and size distribution with composition in bituminous coal of the Western Canadian Sedimentary Basin: implications for coalbed methane potential. Fuel 75, 1483–1498.
6. Fang H., Sang S., Liu S., 2018. A methodology for characterizing the multiscale pores and fractures in anthracite and semi-anthracite coals and its application in analysis of the storage and permeable capacity of coalbed methane. SPE Journal Preprint 23.
7. Flores R., 2014. Coal and coalbed gas: fueling the future. Elsevier, San Diego, USA.
8. Gan H., Nandi S. P., Walter Jr. P. L., 1972. Nature of porosity in American coals. Fuel 51, 272–277.
9. Giffin S., Littke R., Klaver J., Urai J. L., 2013. Application of BIB-SEM technology to characterise macropore morphology in coal. International Journal of Coal Geology 114, 85-95.
10. Harris L. A., Yust C. S., 1979. Ultrafine structure of coal determined by electron microscopy. American Chemical Society. Division of Fuel Chemistry Preprints 24, 210 – 217.
11. Hodot B. B., 1966. Outburst of coal and coalbed gas (Chinese Translation). Beijing: China Industry Press. p. 318.

12. Jettestuen E., Helland J.O., Prodanovic M., 2013. A level set method for simulating capillary-controlled displacements at the pore scale with nonzero contact angles. Water Resources Research, WRCR20334.
13. IUPAC, 1982. Reporting physisorption data for gas/solid systems with special reference to the determination of surface area and porosity. Pure Applied Chemistry 54 (11), pp 2201 –2218.
14. Karachan C. O., Okandan E., 2001. Adsorption and gas transport in coal microstructure: investigation and evaluation by quantitative X-ray CT imaging. Fuel 80, 509-520.
15. Lamberson M. N., Bustin R. M., 1993. Coalbed methane characteristics of the Gates Formation coals, northeastern British Columbia: effect of maceral composition. American Association of Petroleum Geologists Bulletin 77, 2061–2076.
16. Lin W., 2010. Gas sorption and the consequent volumetric and permeability change in coal (PhD dissertation). Palo Alto, California: Stanford University, p. 195.
17. March H., 1987. Adsorption methods to study microporosity in coal and carbons – a critique. Carbon 25, 49 – 58.
18. Mastalerz M., Drobniak A., Strapoc D., Solano Acosta W., Rupp J., 2008. Variations in pore characteristics in high volatile bituminous coals: Implications for coal bed gas content. International Journal of Coal Geology 76, 205 – 216.
19. Moore T. A., 2012. Coalbed methane: a review. International Journal of Coal Geology 101, 36 – 81.
20. Osher S., Sethian J. A., 1988. Fronts propagating with curvature-dependent speed: Algorithms based on Hamilton-Jacobi formulations. Journal of Computational Physics, 79, 12-49.
21. Prodanovic M., Bryant S. L., 2006. A level set method for determining critical curvatures for drainage and imbibition, Journal of Colloid and Interface Science. 304, pp 442–458.
22. Prodanovic M., Lindquist W. B., Seright R. S., 2007. 3D image-based characterization of fluid displacement in a Berea core. Advances in Water Resources 30, pp 214 – 226.
23. Prodanovic M., Bryant S., Karpin Z., 2008. Investigating matrix-fracture transfer via a level set method for drainage and imbibition. SPE Annual Conference and Exhibition held in Denver, Colorado, USA, 21 – 24 September.
24. Prodanovic M., Bryant S., 2009. Physics-driven interface modeling for drainage and imbibition in fractures. SPE Journal, 14, 532–542.
25. Prodanovic M., Bryant S. L., Karpyn Z. T., 2010. Investigating matrix/fracture transfer via a level set method for drainage and imbibition. SPE Journal, 15 (1), pp 125 – 136.
26. Purcell W. R., 1949. Capillary Pressures - Their Measurement Using Mercury and the Calculation of Permeability Therefrom. Society of Petroleum Engineers.

27. Puri R., Evanoff J., Brugler M., 1991. Measurement of coal cleat porosity and relative permeability characteristics. Paper presented at the SPE Gas Technology Symposium, Houston, Texas.
28. Roslin A., Zhou Y., Pokrajac D., Wu K., in press. 3D Pore system reconstruction using nano-scale 2D SEM images and pore size distribution analysis for intermediate rank coal matrix.
29. Sussman M., Smereka P., Osher S., 1994. A level set approach for computing solutions to incompressible two-phase flow. Journal of Computational Physics, 114 (1), pp 146 – 159.
30. Thomas Jr. J., Damberger H. H., 1976. Internal surface area, moisture content and porosity of Illinois coals, variation with coal rank. Circular-Illinois State Geological Survey 493, pp 38.
31. Unsworth J. F., Fowler C. S., Jones L. F., 1989. Moisture in coal 2. Maceral effects on pore structure. Fuel 68, 18–26.
32. Wang H., Yao Y., Liu D., Pan Z., Yang Y., Cai Y., 2016. Fault-sealing capability and its impact on coalbed methane distribution in the Zhengzhuang field, southern Quinshui Basin, North China. Journal of Natural Gas Science and Engineering 28, pp 613 – 625.
33. Wildman J., Derbyshire F., 1991. Origins and functions of macroporosity in activated carbons from coal and wood precursors. Fuel 70, 655 – 661.
34. Wu H., Zhou Y., Yao Y., Liu D., 2019. Imaged based fractal characterization of micro-pore structure in coal sample, Fuel 239, pp 53-62.
35. Wu K., Van Dijke M. I. J., Couples G. D., Sorbie K. S., Ma J., 2006. 3D stochastic modelling of heterogeneous porous media – applications to reservoir rocks. Transport Porous Media 65 (3), pp 443–67.
36. Zhang H., 2001. Genetical type of pores in coal reservoir and its research significance. Journal of China Coal Society 26, 40 – 44.
37. Zhang S., Tang S., Tang D., Pan Z., Yang F., 2010. The characteristics of coal reservoir pores and coal facies in Liulin district, Hedong coal field of China. International Journal of Coal Geology 81, 117 – 127.